Depolarization in diffusely scattering media

Thomas A. Germer

Sensor Science Division
National Institute of Standards and Technology
Gaithersburg, MD 20899 USA

ABSTRACT

We performed Mueller matrix Monte Carlo simulations of the propagation of optical radiation in diffusely scattering media for collimated incidence and report depolarization in the transmitted rays as a function of thickness, the angle subtended by the detector, and the area of the material sampled. This paper expands upon previous work [Germer, J. Opt. Soc. Am A **37** 980 (2020)], whereby it was shown that the complex paths that rays follow serve to depolarize the light and that the measurement geometry is important for obtaining consistent results. In addition, we perform extinction theorem calculations for spheroidal particles and show that for a reasonable distribution of particle eccentricity, the depolarization due to the fluctuations of the diattenuation and birefringence of a solution of such spheroids is insignificant compared to the calculated depolarization induced by scattering.

Keywords: depolarization, modeling, optical theorem, scattering, simulations

1. INTRODUCTION

The evolution of depolarization of optical radiation as it transmits through diffusely scattering media has received considerable recent experimental[1–5] and theoretical[4,6–10] interest. This interest has been spurred by applications that either need to control the polarization in devices or use the depolarization information to gain insight into the character of a medium's inhomogeneity. Such application include biomedical imaging,[11] remote sensing,[12–14] material characterization,[15] and optical devices.[16] Depolarization results from a temporal or spatial random variable that is encountered in the numerous paths that radiation takes in propagating from a source to a detector.

The evolution of the intensity and polarization state of radiation transmitting through a medium is often treated in terms of a 4×4 Mueller matrix $\mathbf{M}(z)$ that evolves according to the differential equation[17–19]

$$\frac{\mathrm{d}\mathbf{M}(z)}{\mathrm{d}z} = \mathbf{m}(z)\mathbf{M}(z), \tag{1}$$

with the initial condition $\mathbf{M}(0) = \mathbf{I}$ (the identity matrix), where $\mathbf{m}$ is a 4×4 differential Mueller matrix, and z is the propagation coordinate. When $\mathbf{m}$ is independent of z, the solution for a layer of thickness Δz is well known:

$$\mathbf{M}(\Delta z) = \exp(\mathbf{m}\Delta z), \tag{2}$$

where the matrix exponential is used.[20] The behavior described by Eq. (2) motivates the logarithmic decomposition of a Mueller matrix,[6,21]

$$\mathbf{L} = \log(\mathbf{M}/M_{00}). \tag{3}$$

When there is no depolarization, $\mathbf{L}$ has the form

$$\mathbf{L}_{\mathrm{nd}} = \begin{pmatrix} 0 & \beta & \gamma & \delta \\ \beta & 0 & \mu & \nu \\ \gamma & -\mu & 0 & \eta \\ \delta & -\nu & -\eta & 0 \end{pmatrix}. \tag{4}$$

Corresponding author: thomas.germer@nist.gov, Telephone: 1 301 975 2876

The remainder, $\mathbf{L}-\mathbf{L}_{\rm nd}$,

$$\mathbf{L}_{\rm dep} = \begin{pmatrix} 0 & \beta' & \gamma' & \delta' \\ -\beta' & \alpha_1 & \mu' & \nu' \\ -\gamma' & \mu' & \alpha_2 & \eta' \\ -\delta' & \nu' & -\eta & \alpha_3 \end{pmatrix}, \tag{5}$$

is entirely depolarizing. Most materials are diagonally depolarizing, meaning the off-diagonal terms in Eq. (5) are zero, and $L_{11}=\alpha_1$, $L_{22}=\alpha_2$, and $L_{33}=\alpha_3$ can be considered measures of depolarization. For isotropic media at normal incidence, $L_{11}=L_{22}$.

Depolarization has often been found to be quadratic with material thickness,[1–3] and in some cases, the observed behavior has been more complicated.[4,5] Two basic approaches have been taken to explain the observed behavior. In the first case,[4,6–8] radiation is treated as propagating forwardly through the medium, experiencing fluctuations in birefringence and diattenuation before leaving the material and reaching the detector. In order to explain the nonlinear evolution of depolarization with thickness, these models rely on those fluctuations having correlation lengths comparable to the thickness of the material. In many cases, such as the construction of a thick material from the stacking of independent uncorrelated layers,[1–3] the assumption that the optical properties are correlated beyond the thickness of one of those layers is suspect.

The present author has considered an alternative approach to understand the evolution of depolarization.[9,10] By considering radiation propagating not only in the forward direction, but also in the backward direction, quadratic and even more complicated behavior can be explained. In the simplest approximation,[9] quadratic behavior in transmission is a result of there needing to be two scattering events for scattered radiation to contribute to the transmittance. When the directional dependence of the scattering is considered,[10] more complex behavior can be observed, especially when very small collection solid angles are considered.

This paper builds upon the work of Ref. 10. In Ref. 10, the measured transmission and its depolarization was investigated in a Monte Carlo (MC) framework as a function of the collection angle. In this work, we investigate the dependence of depolarization on the area from which the rays are collected. Figure 1 shows the virtual measurement configuration. If Ref. 10, all radiation which was emitted within some collection angle β was collected. In this study, we further consider only rays which have been emitted within a radius r. We show that the collection area has a large effect on the measured depolarization. We also perform a simulation of spheroidal particles and use the extinction theorem to show that the depolarization of radiation transmitted normally through the material has significantly less depolarization than that caused by scatter.

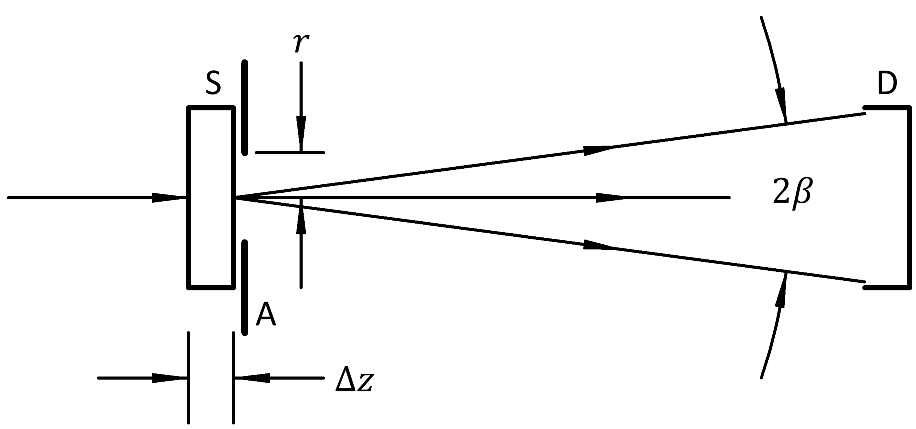

Figure 1. The virtual measurement setup. Radiation strikes a point on material S of thickness Δz, and radiation emitted from the material from an aperture A with radius r and direction within β of the surface normal is collected by detector D.

We describe the MC simulations in Sec. 2. In Sec. 3, we present the results and discuss them. Finally, we make conclusions in Sec. 4.

2. MONTE CARLO MODELING

Monte Carlo modeling was performed using similar methods as those described in Ref. 10. We used polarized phase functions appropriate for spherical particles having index of refraction $n_{\rm sph} = 1.56$ embedded in a medium having index of refraction $n_{\rm water} = 1.33$ and having a log-normal distribution with mean diameters (D_0) of 250 nm and 700 nm and fractional widths $(\Delta D/D_0)$ of 0.5, as well as that appropriate for Rayleigh scattering. The wavelength was 532 nm. These phase functions are shown in Ref. 10. The averages of the cosine of the scattering angle are $g = 0$ for Rayleigh scattering, $g = 0.87$ for the $D_0 = 250$ nm distribution, and $g = 0.93$ for the $D_0 = 700$ nm distribution. The transport mean free path $l_{\rm t}$ is related to the scattering length $l_{\rm s}$ by $l_{\rm t} = l_{\rm s}/(1-g)$.

All lengths in this paper are given in terms of the mean scattering length, $l_{\rm s}$ (that is, $l_{\rm s} = 1$). Rays are initially incident at the origin $(x, y, z) = (0, 0, 0)$ at normal incidence and propagate randomly according to the polarized phase function until they reach either interface at $z = 0$ or $z = \Delta z$. Those rays which reach the boundary $z = \Delta z$ and (a) have a propagation direction subtended by a circular aperture with a half angle β and (b) leave that boundary within a specified radius $r = (x^2 + y^2)^{1/2}$ are collected. For these simulations, we considered $\beta = 1^\circ$, 5°, and 20°. The number of rays propagated for each data point was 2.4×10^8.

For simplicity, we have ignored interface reflections as well as refraction at the entrance and exit of the medium. Furthermore, no absorption, either in the medium surrounding the particles, nor in the particles themselves, was included.

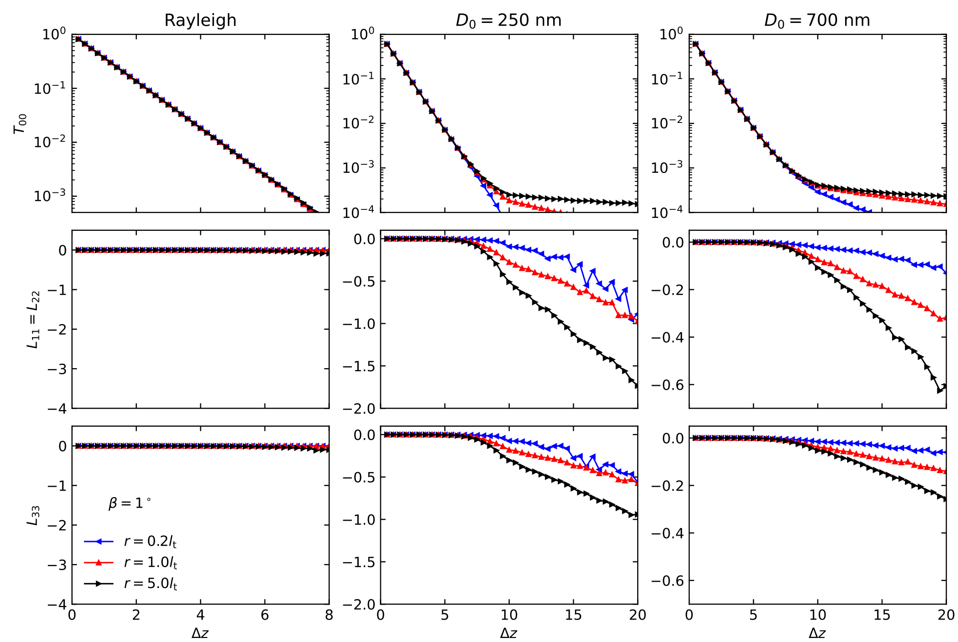

Figure 2. The results of the MC simulations as a function of normalized sample thickness for a collection angle of $\beta = 1^\circ$. The top row shows the effective transmittance M_{00}. The bottom two rows show the non-zero depolarizing logarithmic decomposition elements $L_{11} = L_{22}$ and L_{33}. The phase functions are for (left) Rayleigh, (middle) $D_0 = 250$ nm, and (right) $D_0 = 700$ nm. The areas of collection have radii (blue, left triangles) $r = 0.2l_{\rm t}$, (red, up triangles) $r = l_{\rm t}$, and (black, right triangles) $r = 5l_{\rm t}$.

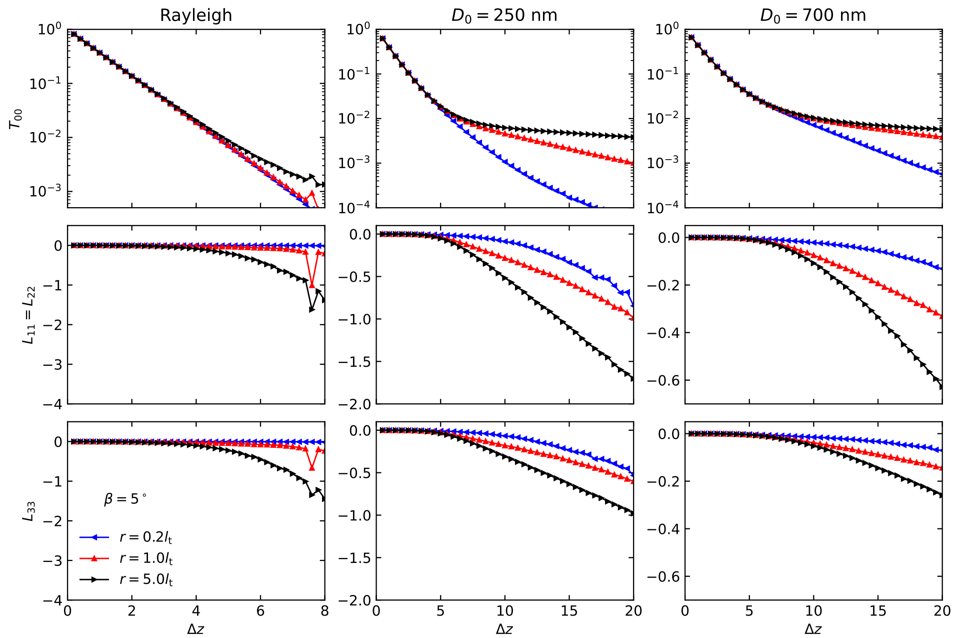

Figure 3. The same as Fig. 2, except for a collection angle of $\beta = 5^\circ$.

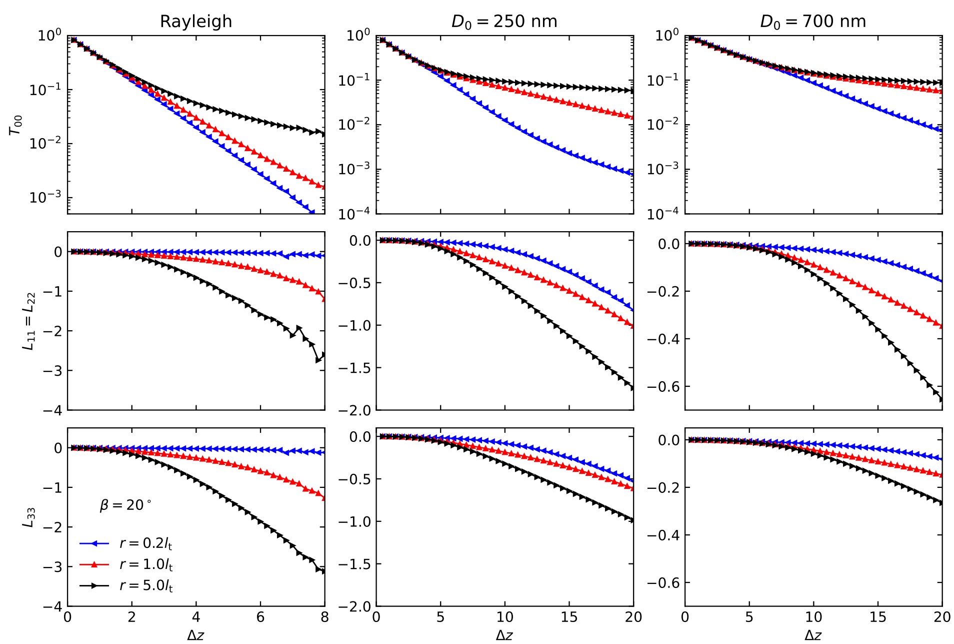

Figure 4. The same as Fig. 2, except for a collection angle of $\beta = 20^\circ$.

3. RESULTS AND DISCUSSION

Figures 2, 3, and 4 show the results of these simulations for $\beta = 1°$, $5°$, and $20°$, respectively. The unpolarized collected transmittance T_{00}, the linear depolarization $L_{11} = L_{22}$, and the circular depolarization L_{33} are each shown as a function of thickness Δz and for three different radii $r = 0.2l_t$, l_t, and $5l_t$ and for each of the three phase functions.

Starting our discussion with the Rayleigh scattering and small collection angle $\beta = 1°$, shown in Fig. 2 (left), the transmittance for all r decay exponentially for all thicknesses and the depolarization is minimal. In fact, the exponential decay rate is $1/l_s$, that is, the scattering rate. For small collection area and angle, the virtual measurement is only selecting those rays that have had little or no scattering. As the collection angles are increased, as seen in Figs. 3(left) and 4(left), deviations from this single-exponential transmittance is increasingly observed, but only when the collection area ($A = \pi r^2$) is increased as well. Depolarization is only observed when the collection angle β and area A allow for capturing light which has been multiply scattered.

Turning our attention to the $D_0 = 250$ nm and $D_0 = 700$ nm phase functions for $\beta = 1°$ (Fig. 2), we observe an initial exponential decay of the transmittance T_{00}, again with the decay rate $1/l_s$, but it levels off at some point, decaying at a second rate that depends upon the collection radius r. The depolarization remains small until that thickness when the transition occurs. That is, when the unscattered rays dominate the total rays collected, little depolarization is observed. For the larger collection angles, $\beta = 5°$ (Fig. 3) and $20°$ (Fig. 4), the level of the diffuse scatter rises according to the area $A = \pi r^2$. As a result, the transition from the transmittance being dominated by unscattered rays to that dominated by diffusely scattered rays and the appearance of depolarization occurs at smaller thickness Δz.

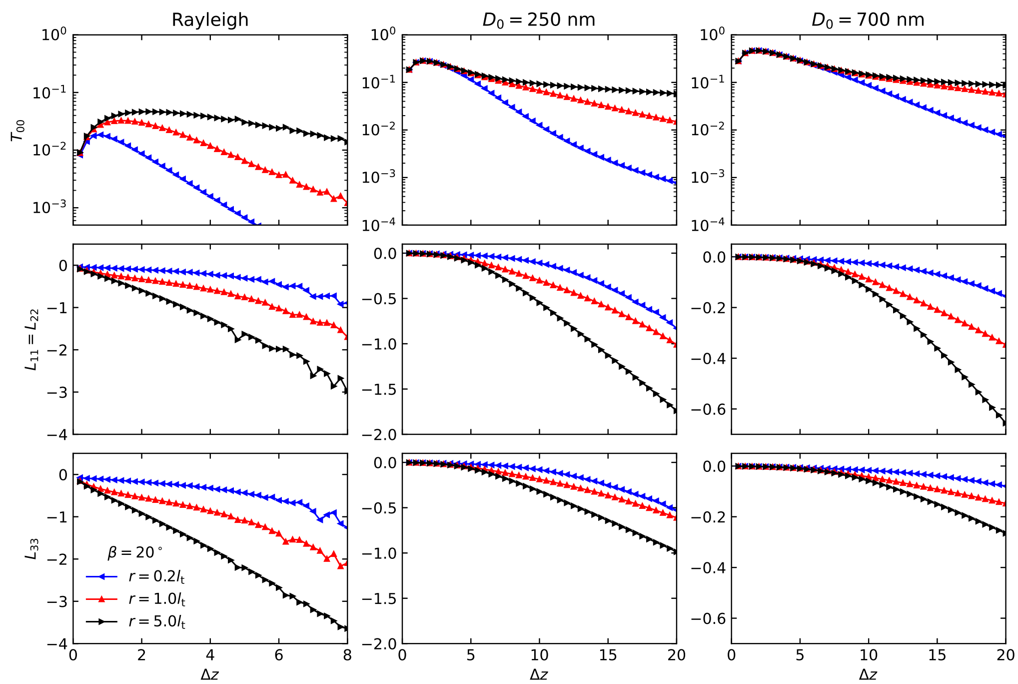

Figure 5. The same as Fig. 2, except for a collection angle of $\beta = 20°$, and unscattered rays were ignored.

Figure 5 shows the scattered transmittance for a collection angle $\beta = 20°$, disregarding unscattered rays. One can notice an initial rise in the transmittance T_{00} for all of the phase functions, followed by a decay as the material gains some opacity. For the Rayleigh phase function, the scattered depolarization appears to decay nearly linearly with thickness. This behavior may seem to contradict the notion that the depolarization resulting from scattering should be quadratic. However, because we are disregarding the unscattered rays in Fig. 5, this initial linear depolarization is resulting from the growing contribution of twice-scattered rays in the simulation. The rise in the scattered transmittance T_{00} is initially linear with thickness. There is very little depolarization in Rayleigh scattering in the forward direction, yet the phase function is such that twice-scattered radiation has usually undergone two large angle scattering events, which are highly depolarizing. For the $D_0 = 250$ nm and $D_0 = 700$ nm particles, the behavior shows small depolarization initially, because the phase functions are forwardly peaked, so a much larger fraction of the twice-scattered rays have undergone two forward scattering events.

The optical theorem relates the forward scattering amplitude to the particle extinction cross section. Karam generalized the optical theorem for the case of anisotropic particles,[22] yielding a differential Mueller matrix extinction cross section. The particles considered in this study, however, were spherical and would exhibit no intrinsic diattenuation or birefringence and thus no variance in those quantities. However, we can make estimates of how large an effect this would be by calculating the effective retardance and diattenuation from axisymmetric spheroids using the T-matrix method.[23,24] We carried out a simulation for spheroids having the same volume distribution as the $D_0 = 250$ nm distribution used above (log-normal distribution of radii), but with eccentricities normally distributed with a standard deviation of 0.1. Each spheroid was averaged over orientation. Using 5000 spheroids, the resulting average differential extinction cross section $\langle \mathbf{C}_{\text{ext}} \rangle$ was found to be diagonal with average cross section $C_{\text{ext}} = 0.063$ μm^2, while the depolarizing part of its variance was found to be

$$\langle \Delta \mathbf{C}^2_{\text{ext}} \rangle = \begin{pmatrix} 0 & 0 & 0 & 0 \\ 0 & -1.1 \times 10^{-7} & 0.08 \times 10^{-7} & 0 \\ 0 & 0.08 \times 10^{-7} & -1.1 \times 10^{-7} & 0 \\ 0 & 0 & 0 & -2.1 \times 10^{-7} \end{pmatrix} \mu\text{m}^4. \tag{6}$$

The logarithmic decomposition in transmission, in the condition of longitudinal homogeneity, is expected to follow[7,8]

$$\mathbf{L} = \frac{N}{V} \langle \mathbf{C}_{\text{ext}} \rangle \Delta z + \frac{N^2}{2V^2} \langle \Delta \mathbf{C}^2_{\text{ext}} \rangle \Delta z^2, \tag{7}$$

where N/V is the number of spheroids per unit volume, which can be adjusted to obtain a given scattering length l_{s} by $l_{\text{s}} = (V/N)/C_{\text{ext}}$. If we evaluate Eq. (7) for $\Delta z = 20 l_{\text{s}}$, the maximum Δz shown in Figs. 2–5, we find that the depolarization matrix has $L_{11} = L_{22} = -5.4 \times 10^{-3}$, $L_{33} = -1.1 \times 10^{-2}$, and $L_{12} = L_{21} = 4 \times 10^{-5}$. Interestingly, there was a significant off-diagonal element $L_{12} = L_{21}$, which results from there being a correlation between the diattenuation and retardance along a given direction, which would be expected for spheroids. The values calculated are insignificant in comparison to the values observed in Figs. 2–4. Since $20 l_{\text{s}}$ is much larger than the scattering length $20 ls$ or the characteristic radius about each particle $[3V/(4\pi N)]^{1/3}$, the depolarization from this contribution is expected to be much less. Thus, the accumulation of depolarization due to the random fluctuations in the local diattenuation and retardance can be neglected.

4. CONCLUSION

In this paper, we expanded upon previous work[9,10] that provided an alternative perspective for the evolution of depolarization in diffuse media. Here, we illustrate how the area that is sampled during the measurement can have a profound impact on depolarization results. For small thicknesses, quadratic depolarization is a natural consequence of diffusion.[9] However, if the measurement weighs the coherent radiation more strongly than the diffuse radiation, either by limiting the solid angle collected by the detector[10] or by limiting the area of the medium from which radiation is collected, the behavior can be significantly more complicated. In addition, we performed calculations using the optical theorem for spheroidal particles, demonstrating that the depolarization from the distribution of spheroids studied would be insignificant compared to that caused by scattering.

REFERENCES

[1] Agarwal, N., Yoon, J., Garcia-Caurel, et al.,"Spatial evolution of depolarization in homogeneous turbid media within the differential Mueller matrix formalism," Opt. Lett. **40**, 5634–5637 (2015).

[2] Yoo, S. H., Ossikovski, R., and Garcia-Caurel, E., "Experimental study of thickness dependence of polarization and depolarization properties of anisotropic turbid media using Mueller matrix polarimetry and differential decomposition," Appl. Surf. Sci. **421** (2017).

[3] Lee, H. R., Yoo, T. S. H., Li, P., et al., "Mueller microscopy of anisotropic scattering media: theory and experiments," in *Unconventional Optical Imaging*, Fournier, C., Georges, M. P., and Popescu, G., eds., Proc. SPIE **10677**, 222–229 (2018).

[4] Charbois, J. M. and Devlaminck, V., "Stochastic model for the differential Mueller matrix of stationary and nonstationary turbid media," J. Opt. Soc. Am. A **33**, 2414–2424 (2016).

[5] Gompf, B., Gill, M., Dressel, M., and Berrier, A., "On the depolarization in granular thin films: a Mueller-matrix approach," J. Opt. Soc. Am. A **35**, 301–308 (2018).

[6] Ossikovski, R., "Differential matrix formalism for depolarizing anisotropic media," Opt. Lett. **36**, 2330–2332 (2011).

[7] Ossikovski, R. and Arteaga, O., "Statistical meaning of the differential Mueller matrix of depolarizing homogeneous media," Opt. Lett. **39**, 4470–4473 (2014).

[8] Devlaminck, V., "Depolarizing differential Mueller matrix of homogeneous media under Gaussian fluctuation hypothesis," J. Opt. Soc. Am. A **32**, 1736–1743 (2015).

[9] Germer, T. A., "Scattering mechanism for quadratic evolution of depolarization," Opt. Lett. **45**, 483–486 (2020).

[10] Germer, T. A., "Evolution of transmitted depolarization in diffusely scattering media," J. Opt. Soc. Am. A **37**, 980–987 (2020).

[11] Pierangelo, A., Benali, A., Antonelli, M.-R., et al.,"Ex-vivo characterization of human colon cancer by Mueller polarimetric imaging," Opt. Express **19**, 1582–1593 (2011).

[12] Bicout, D., Brosseau, C., Martinez, A. S., and Schmitt, J. M., "Depolarization of multiply scattered waves by spherical diffusers: Influence of the size parameter," Phys. Rev. E **49**, 1767–1770 (1994).

[13] Chen, W.-N., Chiang, C.-W., and Nee, J.-B., "Lidar ratio and depolarization ratio for cirrus clouds," Appl. Opt. **41**, 6470–6476 (2002).

[14] Young, A. T., "Revised depolarization corrections for atmospheric extinction," Appl. Opt. **19**, 3427–3428 (1980).

[15] Williams, M. W., "Depolarization and cross polarization in ellipsometry of rough surfaces," Appl. Opt. **25**, 3616–3622 (1986).

[16] Burns, W., Moeller, R., and Chen, C.-L., "Depolarization in a single-mode optical fiber," Journal of Lightwave Technology **1**, 44–50 (1983).

[17] Jones, R. C., "A new calculus for the treatment of optical systems. VIII. Properties of the N-matrices," J. Opt. Soc. Am. **38**, 671–685 (1948).

[18] Azzam, R. M. A., "Propagation of partially polarized light through anisotropic media with or without depolarization: A differential 4×4 matrix calculus," J. Opt. Soc. Am. **68**, 1756–1767 (1978).

[19] Ossikovski, R. and Martino, A. D., "Differential mueller matrix of a depolarizing homogeneous medium and its relation to the mueller matrix logarithm," J. Opt. Soc. Am. A **32**, 343–348 (2015).

[20] Strang, G., *Linear Algebra and Its Applications*, second ed.,p. 205, (Academic Press, New York, 1980).

[21] Ortega-Quijano, N. and Arce-Diego, J. L., "Mueller matrix differential decomposition," Opt. Lett. **36**, 1942–1944 (2011).

[22] Karam, M. A., "Polarimetric optical theorem," J. Opt. Soc. Am. A **15**, 196–201 (1998).

[23] Barber, P. W. and Hill, S. C., *Light Scattering by Particles: Computational Methods*, (World Scientific, Singapore, 1990).

[24] Germer, T. A., "Scatmech: Polarized Light Scattering C++ Class Library." https://pages.nist.gov/SCATMECH/docs/index.htm (2019).